AN ABSTRACT OF THE THESIS OF

Timothy Kean Cummings (Name) for the Master of Science (Degree)

in Oceanography (Major) presented on 16 AUGUST 1973 (Date)

Title: THE MESOSCALE WIND FIELD DURING PROJECT JASIN 1972.

Abstract approved: Redacted for privacy

for Wayne V. Burt

The wind field measured during Project JASIN 1972, a joint British-American venture during September 1972, was analyzed. These measurements were done, with equipment manufactured by Ivar Aanderaa of Bergen, Norway, on large, anchored toroid buoys.

The results of the analysis of the wind field, which included divergence and vorticity estimates and spectral analysis, compared favorably with results from previous studies by other investigators. The spectral analysis of the wind field at different locations showed some differences indicating that ocean wind fields are less homogeneous than had been expected. Basic statistics of the wind speed and direction at the same locations also confirmed this conclusion.

An apparent diurnal cycle in the u and v components of the wind was studied. It was shown that the total wind vector for the study period was quite different at different horizontal locations while hourly

deviations around these means during a day showed remarkable similarities.

A curious eight-hour period found in the divergence estimates on a 100 km grid is possibly related to an eight-hour air pressure wave studied many years ago by Von Hann (1918) and Bartels (1932).

It was concluded that the wind field over the ocean is not entirely homogeneous and some rather large differences are found over a scale as small as 100 kilometers.

The Mesoscale Wind Field During Project JASIN 1972

by

Timothy Kean Cummings

A THESIS

submitted to

Oregon State University

in partial fulfillment of
the requirements for the
degree of

Master of Science

Completed 16 August 1973

Commencement June 1974

APPROVED:

Redacted for privacy

Professor of Oceanography Redacted for privacy
in charge of major

Redacted for privacy

Dean of School of Oceanography

Redacted for privacy

Dean of Graduate School

Date thesis is presented 16 AUGUST 1973

Typed by Cheryl E. Curb for Timothy Kean Cummings

ACKNOWLEDGEMENTS

I wish to thank Professor Henry Charnock, Director of the UK Institute of Oceanographic Services, for inviting Dr. Burt and his group to participate in JASIN 1972, and Dr. Raymond T. Pollard, Coordinator for JASIN 1972, for assistance and encouragement in many ways.

Thanks are also due for the assistance of Asa Robinson, Linda Carey, Lyle Ochs, Joseph Bottero, and Ron Hill for their help, Dr. Rod Mesecar for his help in the design and construction of part of the equipment used, and Dr. Henry Crew and Dr. Clayton A. Paulson for their help in certain aspects of the data analysis.

Special thanks are due Dr. Wayne V. Burt, without whose advice, assistance, and support this thesis would have been impossible.

This research was supported by the Global Atmospheric Research program of the National Science Foundation under Grant GA 28004 and the North Atlantic Treaty Organization under Grant #3(SA-6-5-02 (3) 39 TK).

TABLE OF CONTENTS

LIST OF FIGURES

LIST OF FIGURES (Cont.)

LIST OF TABLES

THE MESOSCALE WIND FIELD DURING PROJECT JASIN 1972

I. INTRODUCTION

The purpose of the present study was to examine the time and space variations in the mesoscale wind field over an open ocean area where topographic effects are negligible when compared to topographic effects over most land areas.

The limits of the mesoscale have been defined differently by a number of authors including Fiedler and Panofsky (1970) and Gray (1972). For this study, the size definition coming into common use in Global Atmospheric Research Program Atlantic Tropical Experiment documents (World Meteorological Organization, 1972) will be used. This places the mesoscale between the cumulus scale and the cloud cluster scale with limits of 10 and 100 kilometers. The time limits of the mesoscale have been defined as ranging from one hour to several days. In this study the time limits used are between ten minutes and the month long extent of the JASIN 1972 study.

Few workers have studied mesoscale processes over land and even fewer over the oceans. For example a recent symposium on air-sea interaction (American Meteorological Society, 1971) had very few papers devoted to mesoscale processes out of the total of 50 papers presented.

Recent attention has been paid to mesoscale processes in an endeavor to help explain larger scale processes (Gray, 1972). Roll (1971) points out the observational difficulties in studying the mesoscale while stressing the importance of mesoscale structures, such as convective cells, in the oceans and the atmosphere. Hsueh (1968) also pointed out the observational difficulties of studying mesoscale eddies over the ocean but was able to define and study eddies ranging in size from a few kilometers to a few tens of kilometers.

Although many authors disagree on the numerical limits of the time and space scales of the mesoscale they all agree on the importance of studying the mesoscale and its interactions with other scales of motion.

The first step in accomplishing this purpose is to set up an adequate observational network. The OSU group decided to concentrate on variations in surface wind velocity and joined the British JASIN 1972 expedition during September 1972 for logistic support. JASIN 1972, which stands for Joint Air-Sea Interaction 1972, involved both British and American scientists, aircraft, ships, and a network of buoys. The study was conducted off the west coast of the Republic of Ireland and was based in the vicinity of Ocean Weather Station Juliet (nominal position 52°30.0'N, 20°0.0'W). A previous JASIN experiment had been conducted during 1970 and the present study was an expansion of that experiment. Details of the previous experiment

are given in Royal Society (1971).

The basic aims of the JASIN experiment were to examine the structure of the air-sea boundary layer to learn more about the fluxes of heat, momentum, and water vapor on time scales up to one month and horizontal space scales up to 100 kilometers (Pollard, 1972). To accomplish this purpose the following program was planned and carried out:

1. Examine the atmospheric boundary layer through vertical soundings.
2. Make spatial and temporal measurements of temperature and currents in the oceanic mixed layer and the seasonal thermocline.
3. Make surface measurements of different parameters from several buoys to allow estimation of fluxes across the air-sea interface and of their horizontal variability.
4. Measure currents in the top few meters of the ocean in the presence of surface waves.
5. Examine vertical gradients of currents and density at the bottom of the oceanic mixed layer and across the seasonal thermocline (Pollard, 1972).

The topic of this thesis is the examination of one aspect of (3), that is the time and space variability of the wind field and the resultant wind stress on the surface. Before explaining how this will be done, the general plans of the experiment will be discussed.

There were five large toroid buoys of the same type used in JASIN 1970 (Royal Society, 1971) in the observational network as illustrated in Figure 1. Buoys B1, D1, and D2 comprised an approximate equilateral triangle 17 kilometers on a side and Buoys B1, A, and B2 comprised an approximate equilateral triangle 100 kilometers on a side. There were three ships which were stationed in the vicinity of Buoys B1, B2, and A. M/V Researcher was stationed at Buoy B1, M/V Discovery was stationed at Buoy A, and Weather Advisor was stationed at Buoy B2. Weather Advisor was also on duty as Ocean Weather Station Juliet. In addition to meteorological instrument packages on each ship and buoy, there were current meters and thermistor chains attached to each buoy. Additional special purpose buoys were also launched from time to time for short periods of time.

On each of the buoys wind speed and vector direction were measured with instruments manufactured by Ivar Aanderaa of Bergen, Norway. The wind direction sensor consisted of a highly damped wind vane and compass system that measured the orientation of the vane relative to the buoy and the orientation of the buoy. Instantaneous direction readings were recorded once during each ten minute sampling interval. The wind speed sensor consisted of a lightweight cup anemometer coupled magnetically to a reduction gear and a potentiometer which in effect counted the number of revolutions of the cups each ten minutes and recorded the integrated wind speed for this

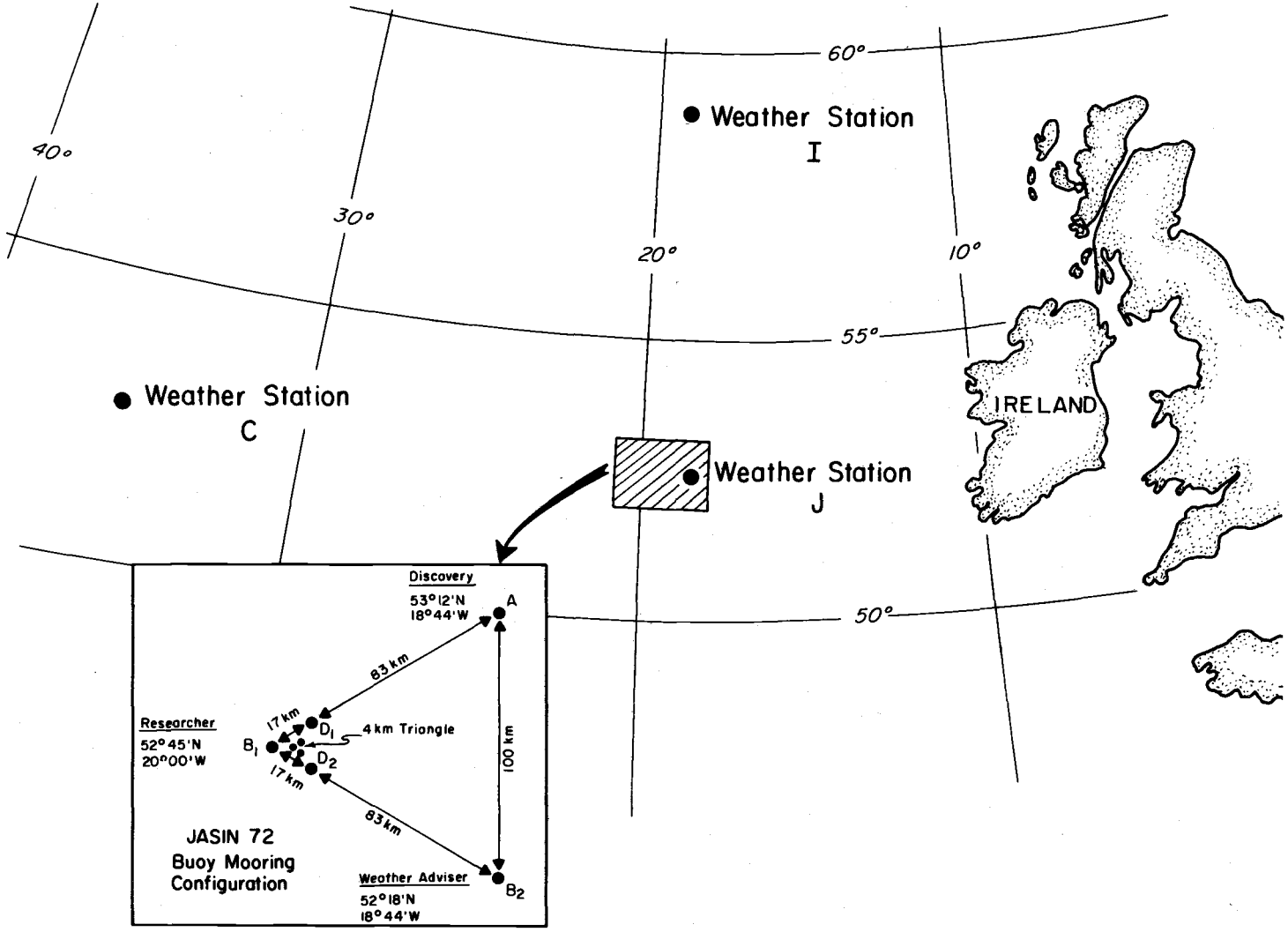

Figure 1. JASIN toroid buoy positions including coast of Ireland and weather ships in vicinity of study area.

period of time.

Data was recorded in a digital form on a 1/4" magnetic tape and was reformatted for reduction on the Oregon State University CDC 3300. In this reduction the data was converted from binary to BCD for easier viewing. Then it was dated with the appropriate month, day, year, and time (GMT). After this it was converted to physical units for the analysis part of the procedure. To insure the security of the data it was saved in both physical units form and raw dated form on 1/2" magnetic tape and stored. The first step in the analysis of the data was to match up wind speeds and vector directions from all five buoys in time. The end result was a continuous record approximately 13 days long where there are readings from all five buoys. The one exception is the wind direction readings from Buoy D1 which are missing except for a continuous 36 hour period and occasional short periods of record during the rest of the 13 days. The following data analyses were carried out on all available data for the 13 day period:

1. Progressive vector diagrams of wind.
2. Basic statistics of wind speed and vector direction.
3. Spectral analysis of ten minute wind speed data.
4. Computation of u-v wind component ellipses.
5. Hourly divergence and vorticity approximations and spectral analysis of same.

II. ENVIRONMENTAL CONDITIONS AND DESCRIPTION OF THE WIND FIELD

Data from the period from the 6th to the 19th of September 1972 was the most useful for the present study. During most of this period, most of the area covered in the JASIN study was dominated by an intense high pressure system. However, several low pressure systems with their associated fronts passed through areas close to the JASIN area and had some effects on the weather within the JASIN area.

Figure 2 shows the air pressure as reported at approximately six hour intervals by Ocean Weather Station Juliet, one of the corner stations of the 100 kilometer triangle constituting the JASIN area. The diagram shows a general increase in pressure during most of the period except for drops in pressure centering about the 6th and 7th, the 15th and 16th, and some time after the 20th. The first drop, on the 6th and 7th of September, was associated with the passage of a weak cold front through the area accompanied by low level cumulus-type clouds and rain showers. Although its effect did not show up on the Juliet pressure records there was an intense low pressure area to the northeast of the JASIN area on the 8th, 9th, and 10th resulting in shower activity in the study area. Because of the presence of disturbances in surrounding areas during most of the study period, the JASIN area was covered by cumulus-type clouds most of the time.

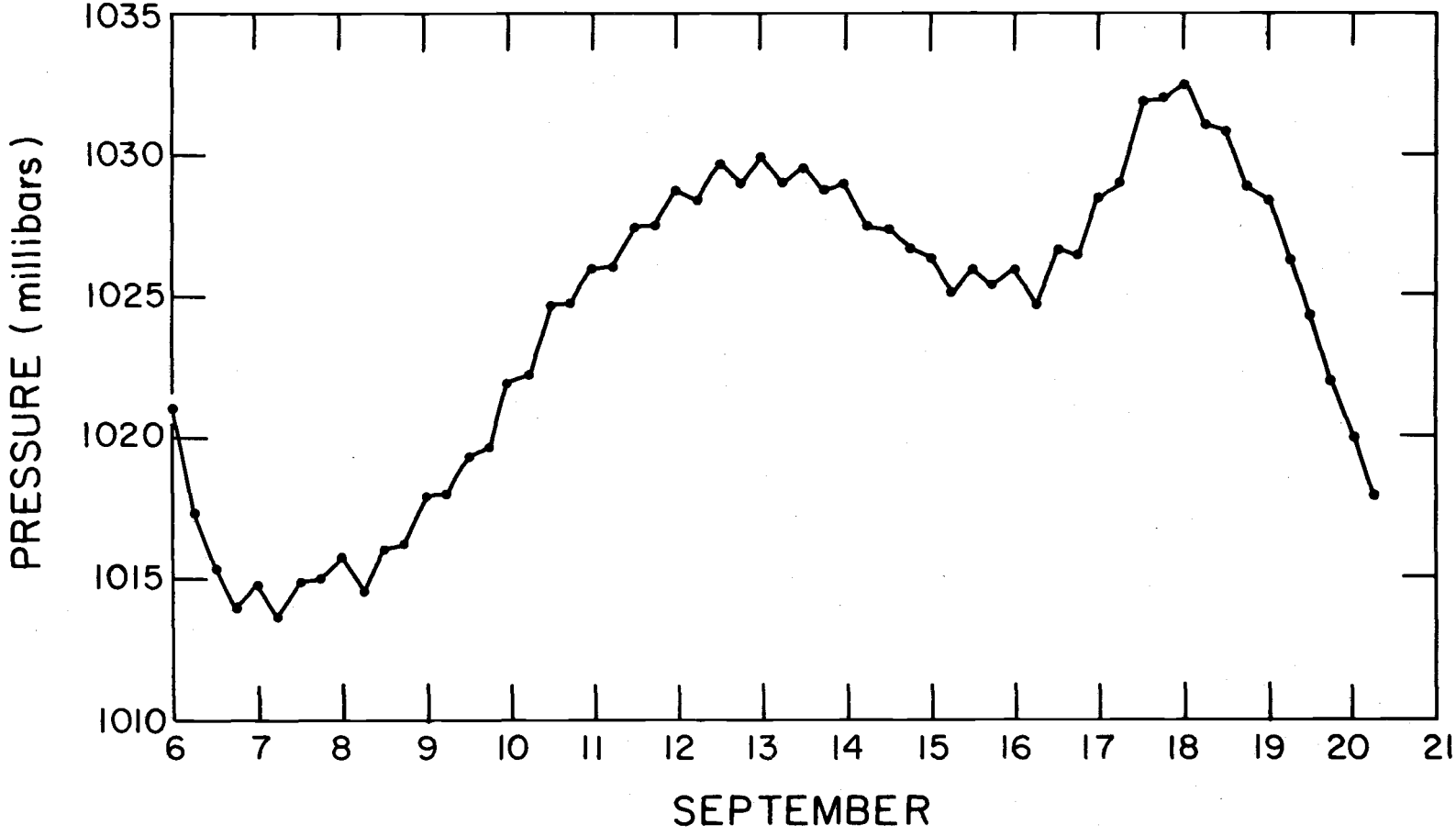

Figure 2. Air pressure record from Ocean Weather Station Juliet for September 6-20, 1972.

The wind fields as measured at all five buoy locations are illustrated with progressive vector diagrams in Figure 3. Some similarities in wind direction and changes in direction are shown at all five locations. There was no prevailing direction. Daily mean wind vector directions varied through all sectors of the compass at all five locations. Table 1 lists the mean vector direction and mean wind speed for each station for each day as well as other statistics on hourly averaged wind speed for the entire study period. Time series of hourly averaged wind speeds are plotted in Figure 4.

For comparison similar wind statistics are shown in Table 2 and Figures 3 and 4 for wind data observed on the research vessel Researcher. The Researcher was stationed in the triangle bounded by Buoys B1, D1, and D2 most of the time. It left this area for the 24 hour period marked "off station" on Figure 4e. It is interesting to note that despite the fact that it is usually considered more difficult to measure winds accurately aboard ship than from an anchored buoy, the directions as measured on the ship showed essentially the same variance as those measured on the buoys, although the ship was almost constantly changing direction and speed throughout the entire period under study. On the other hand the standard deviation of wind speed as measured from the ship was considerably greater than the standard deviations for the buoy wind speeds. However, the mean wind speed as measured on the ship is lower than the mean wind

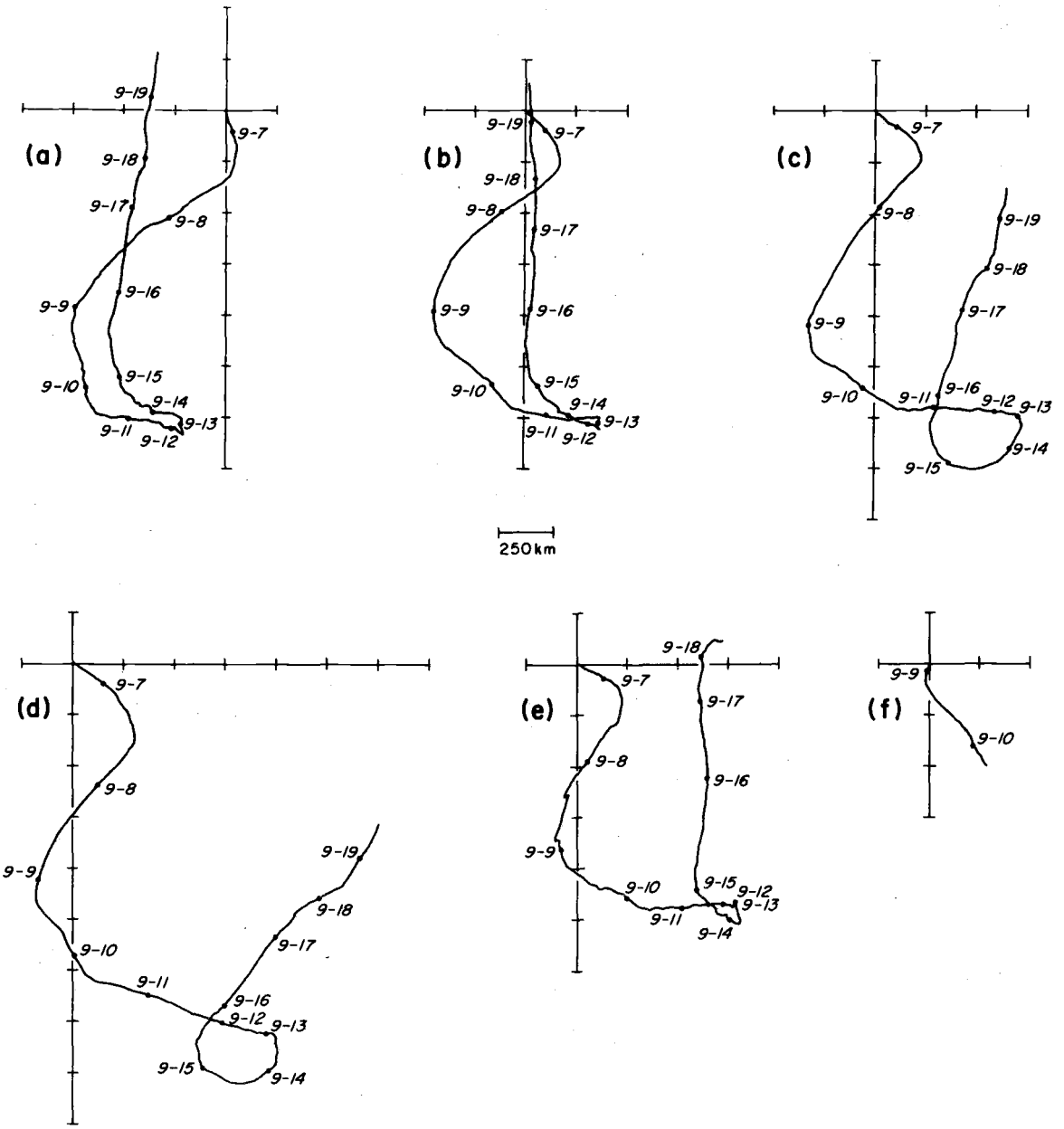

Figure 3. Progressive vector diagrams for wind from (a) Buoy B1, (b) Buoy D2, (c) Buoy B2, (d) Buoy A, (e) M/V Researcher, and (f) Buoy D1.

Table 1. Daily mean vector directions (MD) in degrees and mean wind speeds (MS) in meters/second and basic statistics for the entire study period for Buoys B1, B2, A, D1, and D2.

Date	Buoy B1		Buoy B2		Buoy A		Buoy D1		Buoy D2	
	MD	MS	MD	MS	MD	MS	MD	MS	MD	MS
9/6	165	6.43	126	6.02	125	8.05	---	6.75	133	6.24
9/7	217	7.12	191	6.22	182	7.30	---	7.41	208	6.63
9/8	227	7.71	212	8.12	213	6.74	---	7.20	215	7.44
9/9	173	5.69	138	5.43	153	5.26	151	5.58	140	5.89
9/10	126	4.03	105	4.65	112	5.18	147	4.08	118	3.95
9/11	102	2.89	94	3.84	110	4.69	---	3.34	100	2.77
9/12	64	2.05	101	1.82	103	2.81	---	2.19	87	1.91
9/13	291	2.26	195	2.26	176	2.84	---	2.17	283	2.43
9/14	316	3.40	255	4.00	271	4.16	---	3.51	313	3.14
9/15	359	5.02	351	4.43	18	4.44	---	5.05	353	4.79
9/16	10	4.98	16	5.15	37	4.89	---	5.18	3	4.64
9/17	15	3.02	30	2.97	48	3.48	---	3.65	1	2.89
9/18	6	3.61	14	3.00	46	3.35	---	3.81	355	3.84
9/19	7	6.18	12	4.33	28	5.32	---	6.40	357	5.44

Buoy	Maximum Speed	Minimum Speed	Mean Speed	Standard Deviation
B1	9.09	.81	4.41	1.75
B2	9.05	.91	4.36	1.55
A	11.20	1.05	4.69	1.44
D1	10.28	.82	4.53	1.71
D2	8.85	.89	4.24	1.62

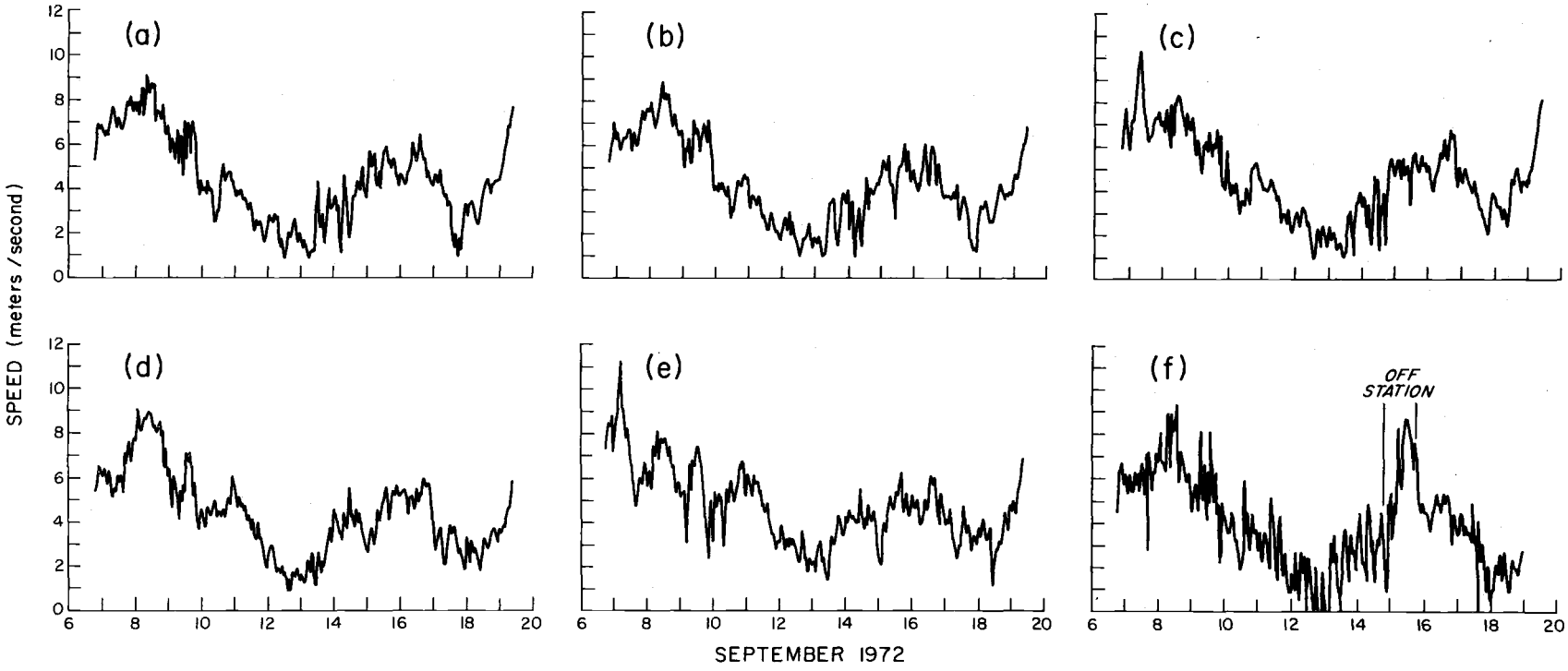

Figure 4. Time series of hourly wind speed averages from (a) Buoy B1, (b) Buoy D2, (c) Buoy D1, (d) Buoy B2, (e) Buoy A, and (f) M/V Researcher.

speeds as measured on the buoys. A reason for this could be the higher threshold for the large heavy wind speed sensor used on Researcher.

Table 2. Daily mean vector directions (MD) in degrees and mean wind speeds (MS) in meters/second and basic statistics for the entire study period for Researcher.

Date	MD	MS
9/6	118	6.04
9/7	187	5.95
9/8	199	7.22
9/10	101	3.51
9/11	86	2.55
9/12	83	1.19
9/13	194	1.99
9/14	311	3.11
9/15	6	6.38
9/16	356	4.49
9/17	0	2.83
9/18	54	2.09

Maximum Speed	Minimum Speed	Mean Speed	Standard Deviation
9.39	0	3.92	1.99

There are many similarities in both speed and direction between the buoy locations as indicated by the progressive vector diagrams and time series of hourly averaged wind speeds. There are also many differences in the two wind parameters. The purpose of the next section will be to examine these differences and similarities more closely.

III. ANALYSIS OF THE WIND FIELD

The first part of this section will be a discussion of the various relationships used in the spectral analysis of the wind field. The second part will be a discussion of the spectral analysis of the horizontal wind speed from all five buoys. The third and last part will be a discussion of the u-v wind component ellipse.

The programs used in estimating the spectral energy of the time series of any physical parameter were developed at the Oregon State University Computer Center. They are all grouped under the OS-3 ARAND System (Ochs et al., 1970 and Ballance et al., 1971) and provide for a variety of time series analyses. It will be useful to go through the various steps that were used for this study to determine the energy spectrum of individual time series.

First a time series, $X(t)$, $t=1, 2, \ldots, N$, is taken and the linear trend is taken out to give a detrended time series, $X_d(t)$, $t=1, 2, \ldots, N$. The form for each individual point in the detrended series is given by,

3-1 $\quad X_d(t)=X(t)-m(t)$, where

3-2 $\quad m(t)=at + b$, $t=1, 2, \ldots, N$.

The coefficients, a and b, are just the slope and intercept of a straight line fitted by a least-squares technique to the original time series. The ARAND routine used for this task has the name DETREND (Ochs et al., 1970). It is important to remove the trend

since distortion can occur in the estimation of spectral energy, particularly at low frequencies, where a time series with a trend is involved (Bendat and Piersol, 1971).

The autocovariance function of the time series, defined by,

$$3\text{-}3 \qquad R(u)=1/N \sum_{t=1}^{N-u} X_d(t)\cdot X_d(t+u),\ u=0, 1, \ldots, u_{max} < N,$$

is computed using a variation of the convolution property of the discrete Fourier transform in conjunction with a fast Fourier transform algorithm (Ballance et al., 1971). The term u_{max} is the maximum truncation point chosen for the data set and is also taken as the number of lags used in computing the autocovariance function. Among the uses of the autocovariance function are its usefulness in examining periodicities in the data. The ARAND routine used in computing the autocovariance function has the name ACFFT (Ballance et al., 1971).

In the next step values of the Fourier coefficients,

$$3\text{-}4 \qquad a(n)=1/N \sum_{t=0}^{2N-1} X_d(t)\cos(\pi\ tn/N) \text{ and}$$

$$3\text{-}5 \qquad b(n)=1/N \sum_{t=0}^{2N-1} X_d(t)\sin(\pi\ tn/N),\ n=0, 1, \ldots, N.$$

are computed using a fast Fourier transform algorithm. The detrended time series is $X_d(t)$, $t=0, 1, \ldots 2N-1$, where $2N$ is the number of data points and must be a power of 2. The ARAND routine used in the computing the Fourier coefficients has the name RCTFFT

(Ochs et al., 1970).

In the present analysis these Fourier coefficients are transformed into spectral energy by the relationship,

$$3\text{-}6 \qquad S(i)=a(i)^2+b(i)^2, \quad i=1,2,\ldots,N,$$

where i=1 is the fundamental frequency, i=N is the Nyquist frequency, and i=2, 3, . . . , N-1 are the harmonics of the fundamental. These estimates are then block averaged with a pseudo-logarithmically increasing bandwidth going towards higher frequencies. Therefore, the averages at low frequencies are crude estimates of the spectral energy while the averages at higher frequencies are better estimates.

The spectral data is then plotted in two different ways. First, the spectral density estimates were plotted on a logarithmic axis versus frequency on a logarithmic axis. Second, the frequency times the spectral density estimates were plotted on a linear axis versus frequency on a logarithmic axis. Both plots are done since they are in common usage in studies with spectral analysis. An advantage of the second type of plot is that equal areas under the curve contribute equally to the variance.

Spectral density estimates were done on unfiltered ten minute wind speed data from Buoys B1, D1, D2, A, and B2. All five time series were matched in time so each had a length of 1828 points which corresponded to a period of almost 13 days. This period went from the 6th to the 19th of September. Measurements from Buoys D1 and

D2 were off five minutes from measurements at the other buoys but this was not a serious problem due to the length of the data record that was used. For each of the cases the detrended time series of wind speed had a small number of zeros added to the end of the series so that the total data length would be a power of 2. This had the effect of slightly reducing the variance of each time series.

The autocovariance functions for all five buoy wind speeds show a general dropoff from the covariance at zero time or zero lags to zero at about 300 lags or 50 hours. The one exception is the wind speed at Buoy A which shows a definite periodicity in the time series of about 27 hours. This autocovariance function is illustrated in Figure 5. The covariance at zero lags for Buoy B1 is 3.33, for Buoy D1 is 3.20, for Buoy D2 is 2.99, for Buoy A is 2.36, and for Buoy B2 is 2.66. It would then appear that there was more variance in the wind speed at the western buoys (B1, D1, and D2) as compared to the wind speed at the eastern buoys (A and B2).

Wind speed spectral plots for Buoys B1, A, and B2 are given in Figure 6. Plots for Buoys D1 and D2 are not included because they were very similar to the wind speed spectral plot from Buoy B1.

The f x S(f) plots all show levels of energy lower than .2 m^2/sec^2 at frequencies higher than 10^{-1} cph. Buoys B1 and B2 have an energy peak at 5×10^{-3} cph while Buoy A has much lower energy

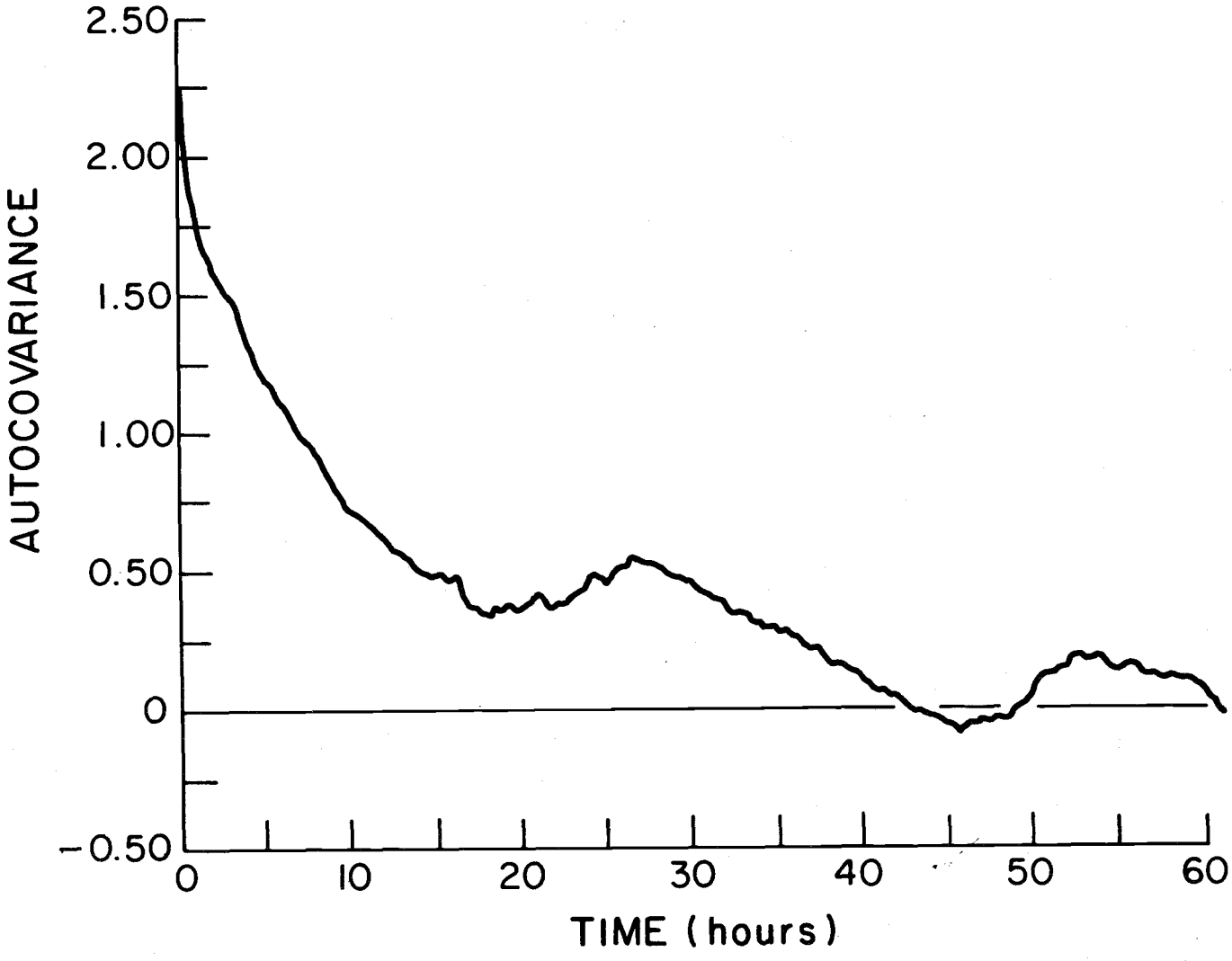

Figure 5. Autocovariance function for ten minute wind speed data from Buoy A.

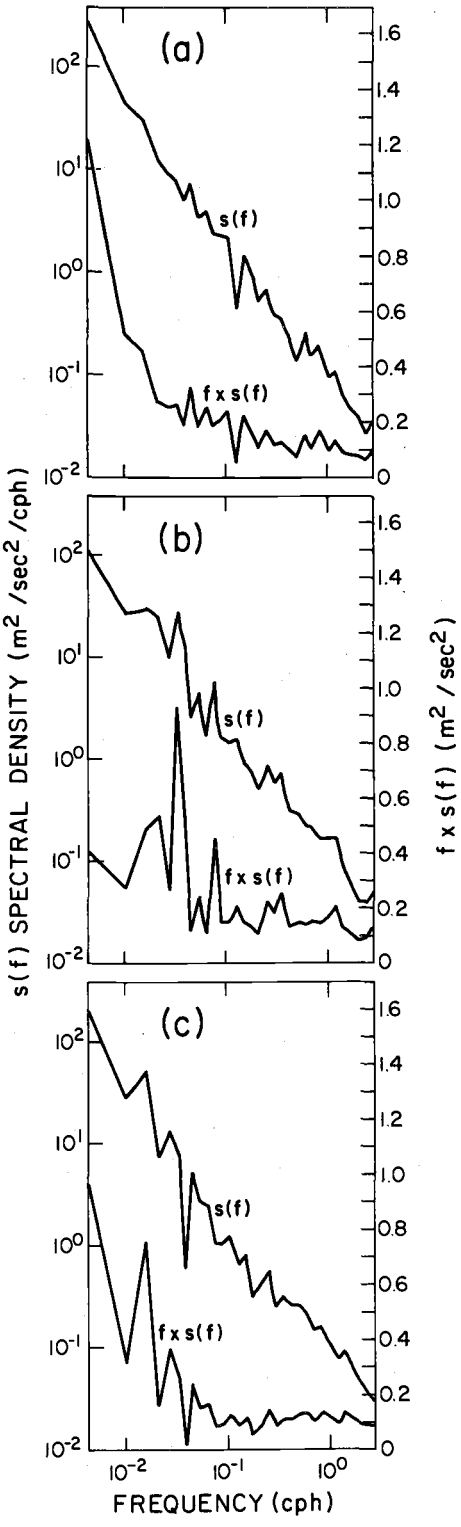

Figure 6. Spectral density and frequency times spectral density for ten minute wind speed data from (a) Buoy B1, (b) Buoy A, and (c) Buoy B2.

levels at that frequency. Instead Buoy A has a peak at 3.33×10^{-2} cph or 30 hours which roughly corresponds to the period of 27 hours found in the autocovariance function. It would appear that Buoys B1 and B2 were influenced by a period in the wind of four to ten days which was missing at Buoy A.

The peaks and gaps in f x S(f) correspond very well with the composite spectrum of wind speed over the sea given by Millard (1971). Millard's spectrum is illustrated in Figure 7. The peak in f x S(f) at 30 hours which occurs at Buoy A is evident in Millard's spectrum but at a higher energy level. In fact the energy levels of the JASIN wind spectrums are all lower than Millard's data, especially at the lower frequencies. Energy levels were relatively higher in Millard's spectrum because he used wind speed measurements taken during the winter. Since the JASIN area was not in any high energy storm tracks, energy in the four to seven day period range is much smaller than the energy levels in Millard's spectrum.

The second part of the analysis of the wind field involved the u and v components of wind, where u is the vector positive to the east and v is the vector positive to the north. On a large scale the changes in the speed and direction were studied using the progressive vector diagrams in Section II. In this section hourly changes in u and v are studied using the u-v ellipse technique.

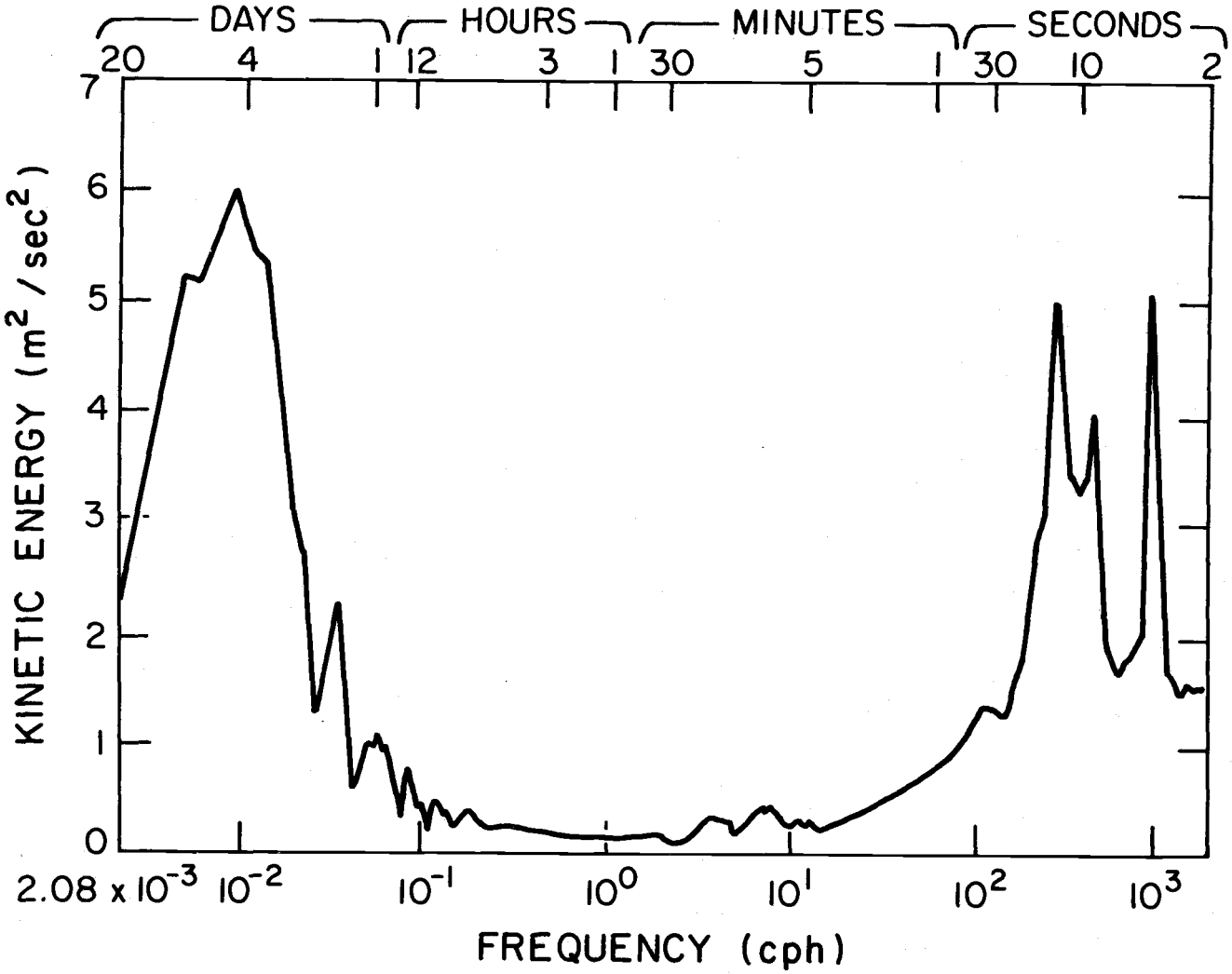

Figure 7. Composite spectrum of wind speed over the sea for periods from 20 days to 2 seconds (Millard, 1968).

First, hourly averages of u and v are taken for each hour of the day during the study period. Then values for each hour of the day were averaged for the study period. The end result was 24 pairs of u and v values, one for each hour of the day. Each set of values seemed to exhibit a 24 hour periodicity so a sinusoidal curve with a 24 hour period was fitted using a least-squares technique to each of the data sets. Then for each hour of the day pairs of u and v fitted values are plotted on a two-dimensional surface with u as the x-axis and v as the y-axis. The end result of the 24 plotted points is an ellipse, from which such things as the eccentricity, major axis, minor axis, and rotation of major axis can be computed. The resulting u-v ellipses for the wind from Buoys B1, D2, A, and B2 plus an insert map of the relative locations of the buoys are given in Figure 8.

The form of the ellipses are very similar for all four buoys with the eccentricity larger for Buoys B2 and A than for Buoys B1 and D2. The mean wind vector for Buoy B1 is to the northwest while that for Buoy D2 is practically zero. The mean wind vector for the other two buoys is to the southeast but the magnitude of the vector for Buoy A is larger than that for Buoy B2. There appears to be some sort of gradient in the mean vector direction and magnitude, and the eccentricity of the wind ellipse in a roughly northeast-southwest line. While the mean wind vector direction and magnitude are different for each buoy the hourly variations around the mean are very similar for

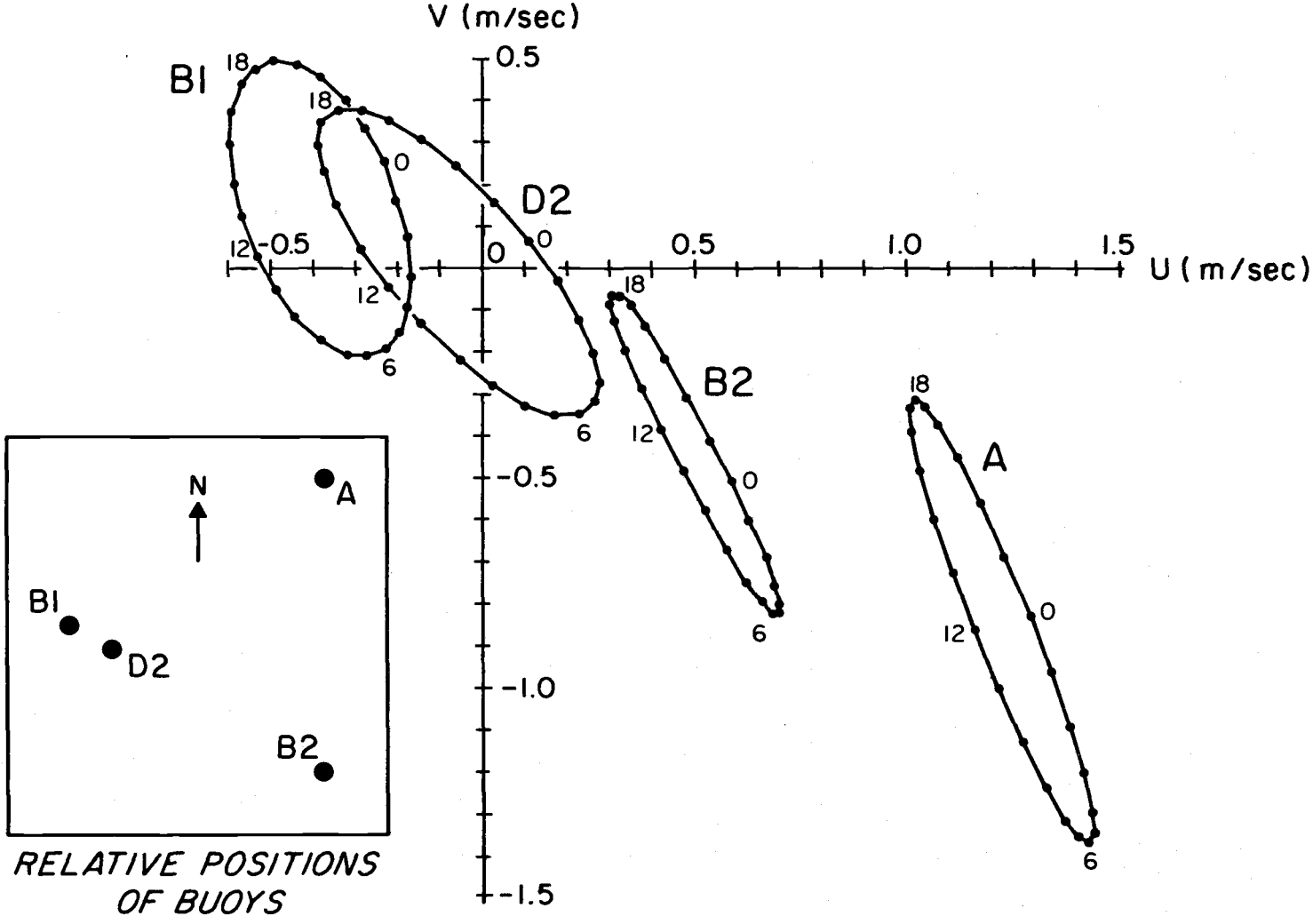

Figure 8. U-V wind component ellipses from Buoys B1, D2, A, and B2 plus an insert map of the relative locations of the four buoys.

all buoys. It is interesting to note that though there was a 24 hour periodicity in the u and v components of the wind, spectra of the horizontal wind speed did not show a large amount of energy at that period. Wind vector direction then played a significant role in showing a 24 hour periodicity in the wind data.

The next topic of the thesis will be a discussion of the divergence and vorticity of the horizontal wind field during JASIN 1972.

IV. DIVERGENCE AND VORTICITY

During the JASIN 1972 experiment there was a unique opportunity to study the horizontal divergence and the vertical component of vorticity of the surface wind field over the oceans where there are no orographic effects due to land terrain features, and no troublesome corrections are necessary for differences in elevation of the locations where observations are made. As Schaffer (1973) points out the latter corrections are particularly difficult to make and the results are difficult to interpret.

There have been very few studies of divergence and vorticity in the mesoscale and none that we know of have been carried out over the oceans due to the lack of observation stations with the proper spacing.

Two grid scales were used in the analysis. Each grid involved a triangular array of three buoys (see Figure 1). The smaller grid, an approximate equilateral triangle, had buoy spacing of 17 kilometers and consisted of Buoys B1, D1, and D2. There were 36 hours of continuous simultaneous wind observations available for analysis from all three of these buoys.

The larger grid formed an approximate equilateral triangle with buoy spacing of 100 kilometers and consisted of Buoys B1, B2, and A. There were 303 hours of continuous simultaneous wind observations available for analysis from all three of these buoys.

Because of the magnitude of difference in size of the two grids we were able to look at two different subscales of motion and compute divergence and vorticity for each subscale.

It has been stated previously (Petterssen, 1956) that planetary waves have a mean divergence of the order 10^{-6} sec^{-1}, synoptic motions of the order 10^{-5} sec^{-1}, and subsynoptic motions of the order 10^{-4} sec^{-1}. Haltiner and Martin (1957) referring to Panofsky (1946) state that the mean horizontal divergence measured over a grid scale L (in meters) can have an order of magnitude of 1/L. Since the order of magnitude of divergence can change over various scales of motion, it can also be possible that vorticity can have approximately the same orders of magnitude over the same scales of motion. If the 1/L relationship is true, one can expect the following orders of magnitude in divergence (and possibly vorticity): for the 17 kilometer triangle 10^{-4} sec^{-1}, and for the 100 kilometer triangle 10^{-5} sec^{-1}. The present study will attempt to verify these orders of magnitude and examine temporal fluctuations of divergence and vorticity through spectral analysis.

By definition the equation of divergence is given by,

$$4\text{-}1 \qquad D = \nabla \cdot \vec{V} = \frac{\partial u}{\partial x} + \frac{\partial v}{\partial y} + \frac{\partial w}{\partial z},$$

where u is the wind vector component in the x-direction or to the east, v is the wind vector component in the y-direction or to the north, and

w is the wind vector component in the z-direction or in the vertical pointed upwards (Petterssen, 1956). Since vertical velocity was not measured the horizontal divergence was used which is defined by,

$$4\text{-}2 \qquad D_h = \nabla_h \cdot \vec{V} = \frac{\partial u}{\partial x} + \frac{\partial v}{\partial y} \ .$$

The horizontal divergence is positive for horizontally expanding (or vertically sinking) flow and negative for horizontally contracting (or vertically rising) flow.

The equation for vorticity is given by,

$$4\text{-}3 \qquad V = \nabla \times \vec{V},$$

where only the vertical component is used in the present study. This is given by,

$$4\text{-}4 \qquad \xi = \frac{\partial v}{\partial x} - \frac{\partial u}{\partial y} ,$$

where the terms are defined already (Haltiner and Martin, 1957). The vorticity is positive for cyclonic (or anticlockwise) flow and negative for anticyclonic (or clockwise) flow.

It is possible to use several different grids to approximate the divergence and vorticity using Equations 4-2 and 4-4. For this study an equilateral triangle grid was used because of the positions of the moored buoys. This presented no problems in estimating the divergence and vorticity of the horizontal wind field but some assumptions were made. First, it was assumed that both grids were equilateral

triangles. The second assumption was that the larger triangle had sides of exactly 100 kilometers and the smaller had sides of exactly 17 kilometers. The proposed mooring diagram for this experiment is illustrated in Figure 1 but the positions may be slightly in error due to small errors in navigation.

If a sample equilateral triangle grid is taken, it can be illustrated how divergence and vorticity were calculated. First, a grid was set up with each corner assigned a number from one to three. These three corners were to represent each of three buoys in the triangular grid. For each of these three corners there would be N sets of wind observations (speed and vector direction) which would be matched in time with those of the other corners. The one exception is the 17 kilometer triangle where the measurements from Buoys D1 and D2 were off five minutes from the measurements at Buoy B1. This was not a serious problem since the general character of the wind field did not appear to change much over a five minute period during the course of the study. The orientation of the grid to true north had to be determined so that the wind component vectors could be computed properly. It was assumed for this experiment that the line connecting Buoys D1 and D2 and the line connecting Buoys A and B2 were in north-south orientations. This sample grid is illustrated in Figure 9a with a sample wind vector and the u and v components for each corner.

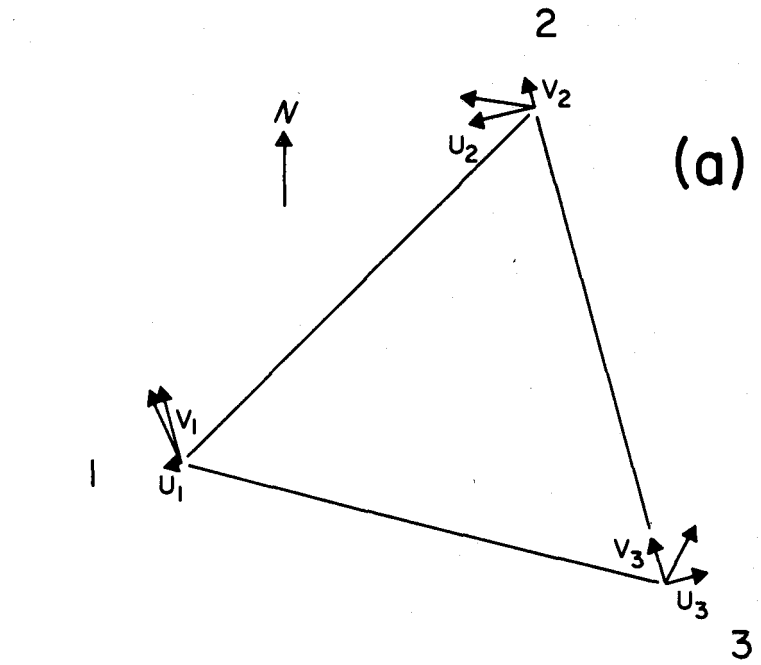

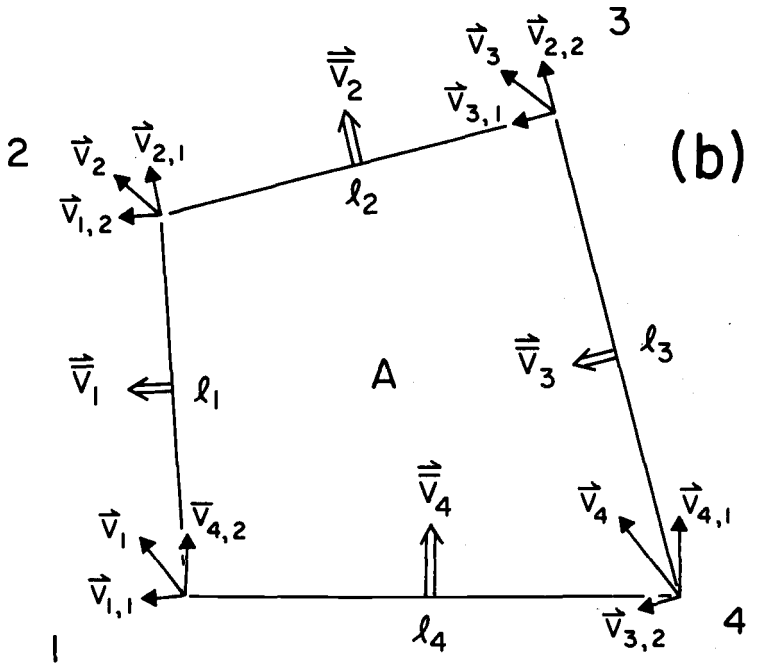

Figure 9. (a) Equilateral triangle buoy arrangement with a sample wind component diagram for each corner and (b) Polygonal buoy arrangement with a sample wind component diagram for each corner and face.

The four terms $\frac{\partial u}{\partial x}$, $\frac{\partial v}{\partial y}$, $\frac{\partial v}{\partial x}$, and $\frac{\partial u}{\partial y}$ are then needed for the computation of vorticity and divergence. The computational forms of the four terms are given below.

4-5 $$\frac{\partial u}{\partial x} \approx \left[\frac{u_2 + u_3}{2} - u_1\right] /x$$

4-6 $$\frac{\partial v}{\partial y} \approx (v_2 - v_3) /y$$

4-7 $$\frac{\partial v}{\partial x} \approx \left[\frac{v_2 + v_3}{2} - v_1\right] /x$$

4-8 $$\frac{\partial u}{\partial y} \approx (u_2 - u_3) /y$$

y is the length of the side of the triangle and x is obtained through geometry.

By combining Equations 4-2, 4-5, and 4-6 the formula for divergence is given by,

4-9 $$D_h = \frac{\partial u}{\partial x} + \frac{\partial v}{\partial y} \approx \left[\frac{u_2 + u_3}{2} - 1\right] /x + (v_2 - v_3)/y.$$

By combining Equations 4-4, 4-7, and 4-8 the formula for vorticity is given by,

4-10 $$\xi = \frac{\partial v}{\partial x} - \frac{\partial u}{\partial y} \approx \left[\frac{v_2 + v_3}{2} - v_1\right] /x - (u_2 - u_3)/y.$$

The computer program that was developed to compute divergence and vorticity for an equilateral triangle grid using Equations 4-9 and 4-10 is in the Appendix under the name VORT (Cummings, 1973).

A secondary means of calculating divergence was developed so networks of buoys that numbered three or more that were in any configuration could be used. By another definition the divergence of the wind field is given by,

$$4\text{-}11 \qquad D = \nabla \cdot \vec{V} = \underset{V \to O}{\text{LIM}} \int_S n \vec{V} dS ,$$

where V is the volume of a particle of air, n is the normal vector, $\vec{V}$ is the normal wind vector, and dS is an increment of area on the surface of the volume (Streeter, 1966).

If there is a polygonal buoy arrangement of k buoys with each pair of buoys separated by a distance l_i, i=1,k, and the wind sensors all fixed at a height, z_o, above the sea surface, then the divergence can be computed. If the vertical components of velocity are considered negligible then Equation 4-11 becomes,

$$4\text{-}12 \qquad D_h = 1/V \sum_{i=1}^{K} \vec{v}_i S_i , \text{ where}$$

$$4\text{-}13 \qquad S_i = l_i z_o \text{ and}$$

$$4\text{-}14 \qquad V = A z_o .$$

A is the area that the buoys bound on the sea surface and $\vec{v}_i$, i=1,k, are the normal wind vectors out of each face. If it is possible to approximate these normal wind vectors then combining Equations 4-12, 4-13, and 4-14 will give,

$$4\text{-}15 \qquad D_h = 1/A \sum_{i=1}^{K} \vec{v}_i l_i$$

How Equation 4-15 can be used is illustrated with the help of Figure 9b (with a sample wind vector component diagram for each face). It is also important to know the orientation of each face with respect to true north so the normal wind vectors for each face can be computed. The normal wind vector for each face is actually taken as an average of the normal vectors on the two corners bounding each face. This is also illustrated in Figure 9b.

The computer program that uses Equation 4-15 to compute divergence is in the Appendix under the name DIVCONV (Cummings, 1973). It should be noted that the two methods of computing the divergence give exactly the same results.

A different means of spectral analysis was used on the divergence and vorticity estimates than was used in Section III. The detrending procedure and computation of the autocovariance function was done as before. However, from this point, values of the spectral density function are estimated using values of the autocovariance function of the time series. The first step in this procedure is to determine the weights for a Tukey or Cosine lag window. These weights are then used to average the spectral estimates, which are defined by,

$$4\text{-}16 \qquad S(f) = 2\left[R(0) + \sum_{u=1}^{m-1} R(u) \cdot w(u/m) \cdot \cos(2\pi fu) \right], \text{ where}$$

w(u/m) are the weights of the Tukey lag window and m is the

truncation point or the maximum number of lags(u). Spectral estimates are determined over the frequency interval 0 to 1/2. These units of frequency are cycles per sampling interval. The ARAND routine used in estimating the spectral density has the name TRANFR (Ochs et al., 1970).

In addition multiplicative factors used in determining confidence intervals for spectral estimates computed indirectly by transforming an autocovariance function are computed. These confidence intervals are either the 80% of 95% confidence limits for a chi-squared test on the spectral data. The ARAND routine used in estimating these factors has the name CONFID (Ochs et al., 1970).

This method of spectral analysis was not used on the wind speed data in Section III because there was a bias using this system causing shifts in energy peaks and increases in energy. This method used with the divergence and vorticity data did not exhibit this bias.

Spectrums of the ten minute divergence and vorticity data showed several peaks at higher frequencies which could have been due to aliasing of wind direction and buoy motion. Because of this, hourly averages of wind speed and vector direction were taken, and divergence and vorticity were computed from these values in an attempt to filter out high frequency energy. It was particularly important to filter direction since these instantaneous readings may be prone to errors. This is so since direction is a sum of two vectors (wind

direction relative to a compass reading) which are both influenced by the motion of the toroid buoy. It should be kept in mind, however, that both the wind vanes and compasses were heavily damped.

Another possible problem with direction readings involves the exact alignment of the two vector sensors. An example was studied to see how serious this problem might be. From the ten minute 100 kilometer triangle wind observations one buoy was chosen and its wind vector direction readings were increased by five degrees for the first case and 20 degrees for the second case. The divergence was then recomputed for this grid using both sets of new directions. The forms of the resulting time series of divergence were very similar to the original series. However, for the plus five degrees case, the mean decreased by 1.8% while the standard deviation increased by 3.6%. For the plus 20 degrees case the mean decreases by 10.8% while the standard deviation increased by 19.6%. For this study this was no problem since the alignment errors were never more than five degrees.

No spectrums were computed for the 17 kilometer triangle hourly divergence and vorticity estimates since the sample size of 36 readings was too small. Therefore, spectral estimates were done only for the 100 kilometer triangle divergence and vorticity estimates. The time series of divergence and vorticity used in computing the spectrums are illustrated in Figure 10. The autocovariance functions

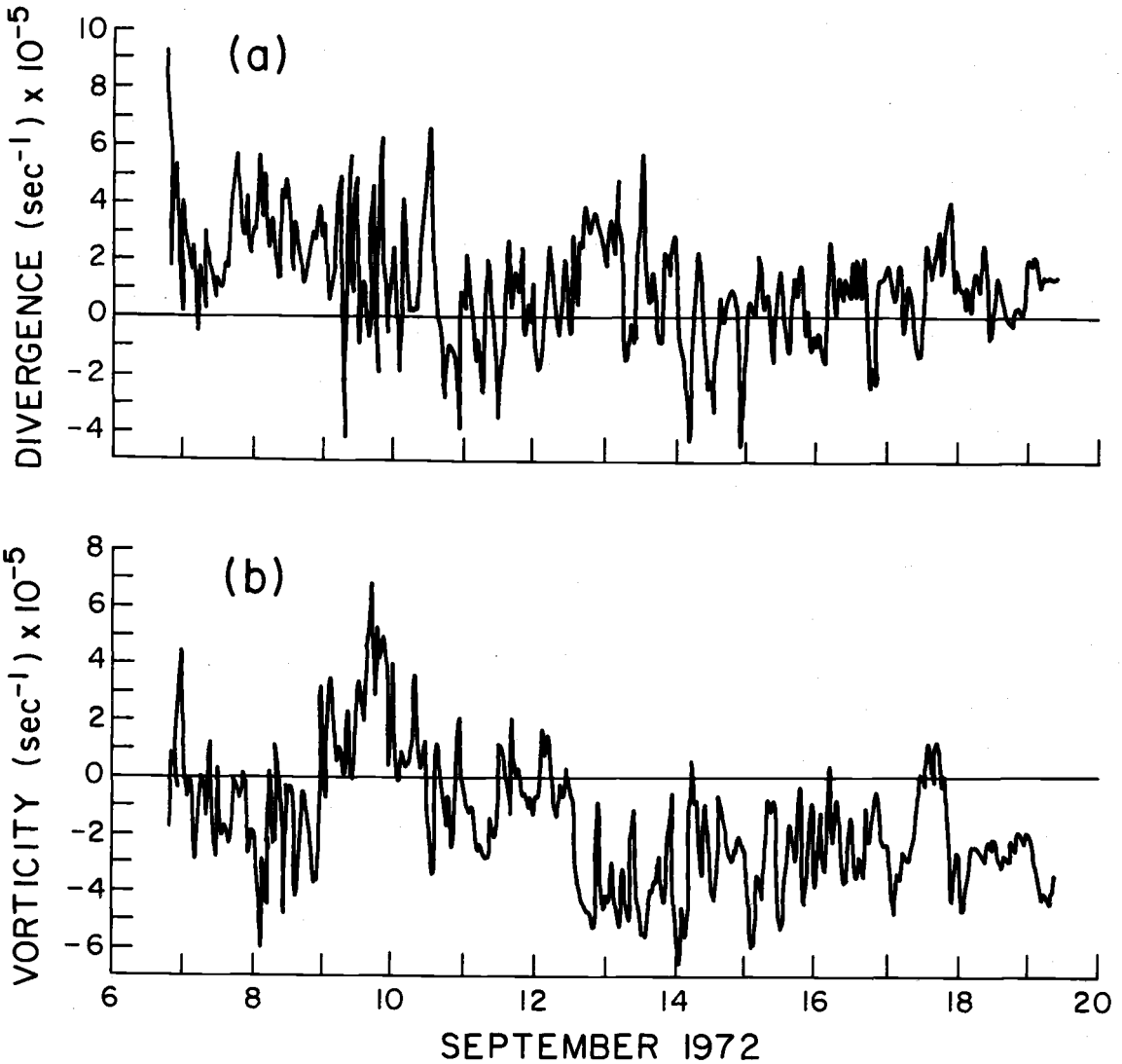

Figure 10. Time series of (a) hourly divergence estimates and (b) hourly vorticity estimates from 100 km triangle.

of divergence and vorticity are illustrated in Figure 11, and the spectral energy estimates for divergence and vorticity are illustrated in Figure 12.

The autocovariance function for vorticity shows no real pattern while that for divergence shows a distinctive period in the measurements of eight to ten hours. The spectrum of divergence also shows a peak in that same period range. There is a slight peak in the same period range in the vorticity spectrum but the 95% confidence bars are much larger, indicating that peak may not be significant. There is a peak in the vorticity spectrum which is centered at .25 cph which corresponds to a period of four hours. It is possible that this peak is the result of aliasing. Because of the large bandwidth in the divergence spectrum the peak of energy in the period range of eight to ten hours can actually be a sum of several peaks and gaps with a major peak somewhere in that period range. Even though the divergence estimates have been filtered spectrums of that parameter can still have aliased peaks of energy, some of them within the eight to ten hour period range.

In looking for a possible cause of a peak of energy in the divergence spectrum at eight to ten hours (other than aliasing), Lettau (1973) mentions the possibility of pressure gradients being the cause while having no apparent effect on vorticity. A distinctive eight hour wave of pressure had been investigated by Von Hann (1918), Bartels

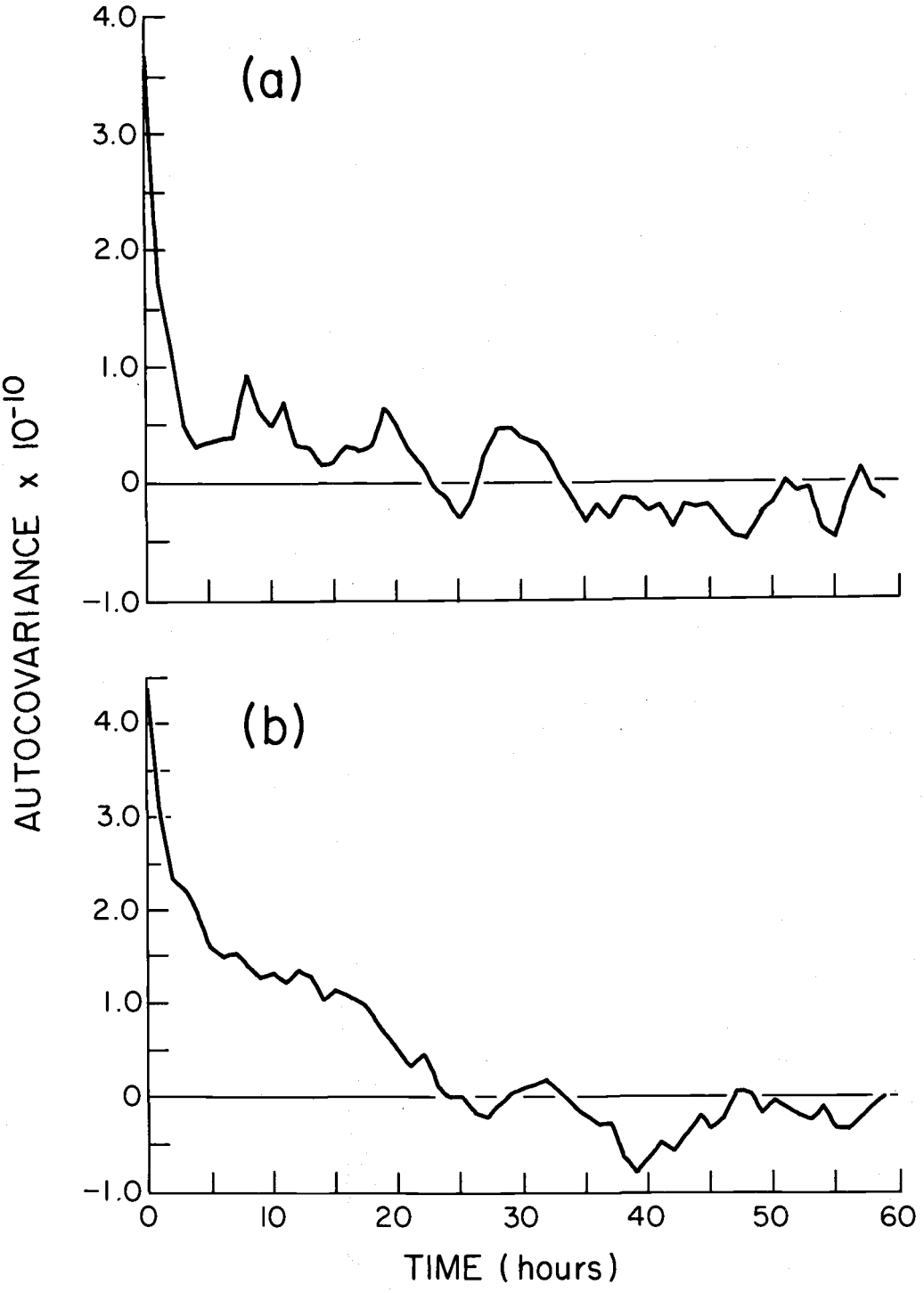

Figure 11. Autocovariance functions for (a) hourly divergence estimates and (b) hourly vorticity estimates from 100 km triangle.

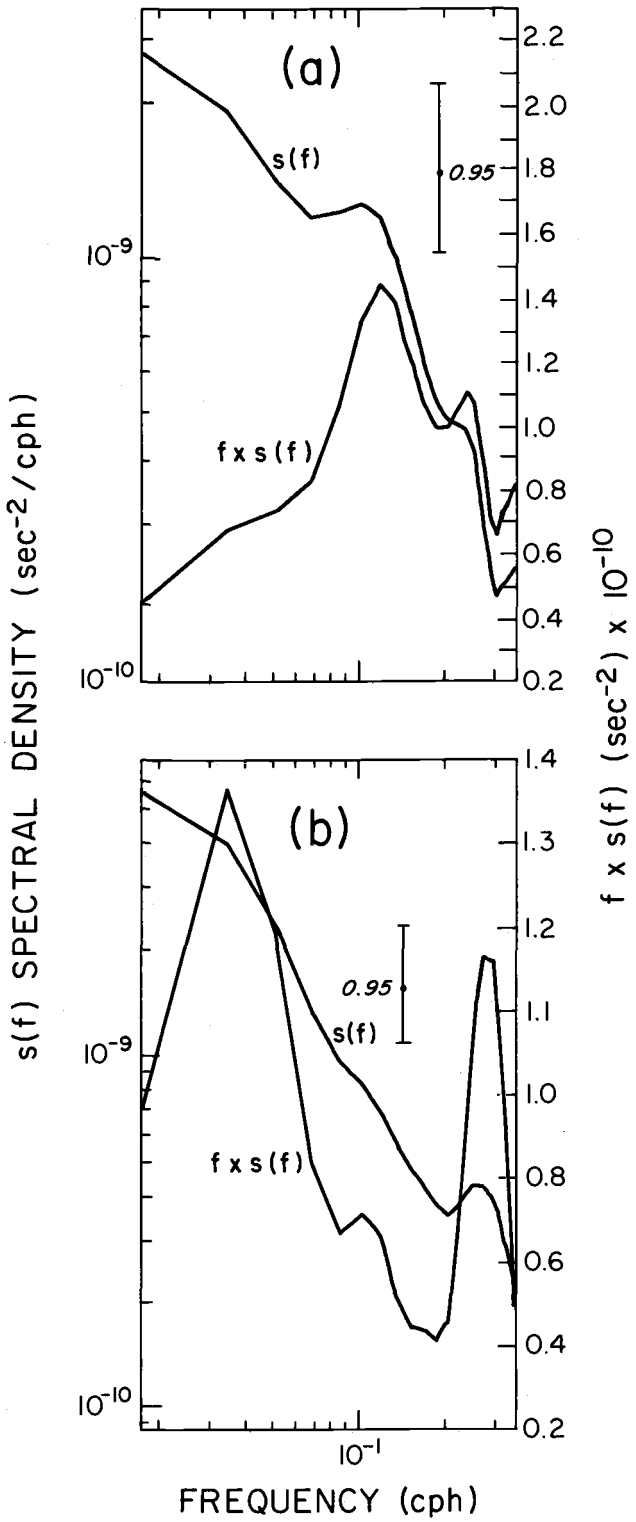

Figure 12. Spectral density (plus 95% confidence limits) and frequency times spectral density for (a) hourly divergence estimates, and (b) hourly vorticity estimates from 100 km triangle.

(1932), and Bartels (1938). Their studies stem from an investigation of atmospheric tides caused by solar and lunar sources. These solar-caused tides have a characteristic motion that can be the sum of a number of sine waves with periods of a day and the various harmonics of a day (12 hours, 8 hours, 6 hours, etc.). The examination of these tides involved taking atmospheric pressure records and doing a harmonic analysis on them. This harmonic analysis just takes physical data and fits a number of sine curves of different periods, the sum of which approximates the original curve.

Bartels (1938) suggests preparing pressure data for harmonic analysis by first taking averages for each hour of the day for a period of about a month. The result is 24 values, one for each hour of the day. This data should then have any trend taken out if the study period is during a climatic transition. The harmonic analysis is then done using a least-squares technique. This analysis was done for the hourly pressure data from M/V Researcher so some comparison with divergence could be done. The complete pressure record is illustrated in Figure 13. The harmonic analysis was done on the Oregon State University School of Oceanography PDP-15. The output for the harmonic analysis for 24, 12, and 8 hour periods using detrended data is shown in Figure 14. Before going into a discussion of the data from the harmonic analysis a short discussion of the eight hour wave of pressure may be in order. This will be the only wave of pressure

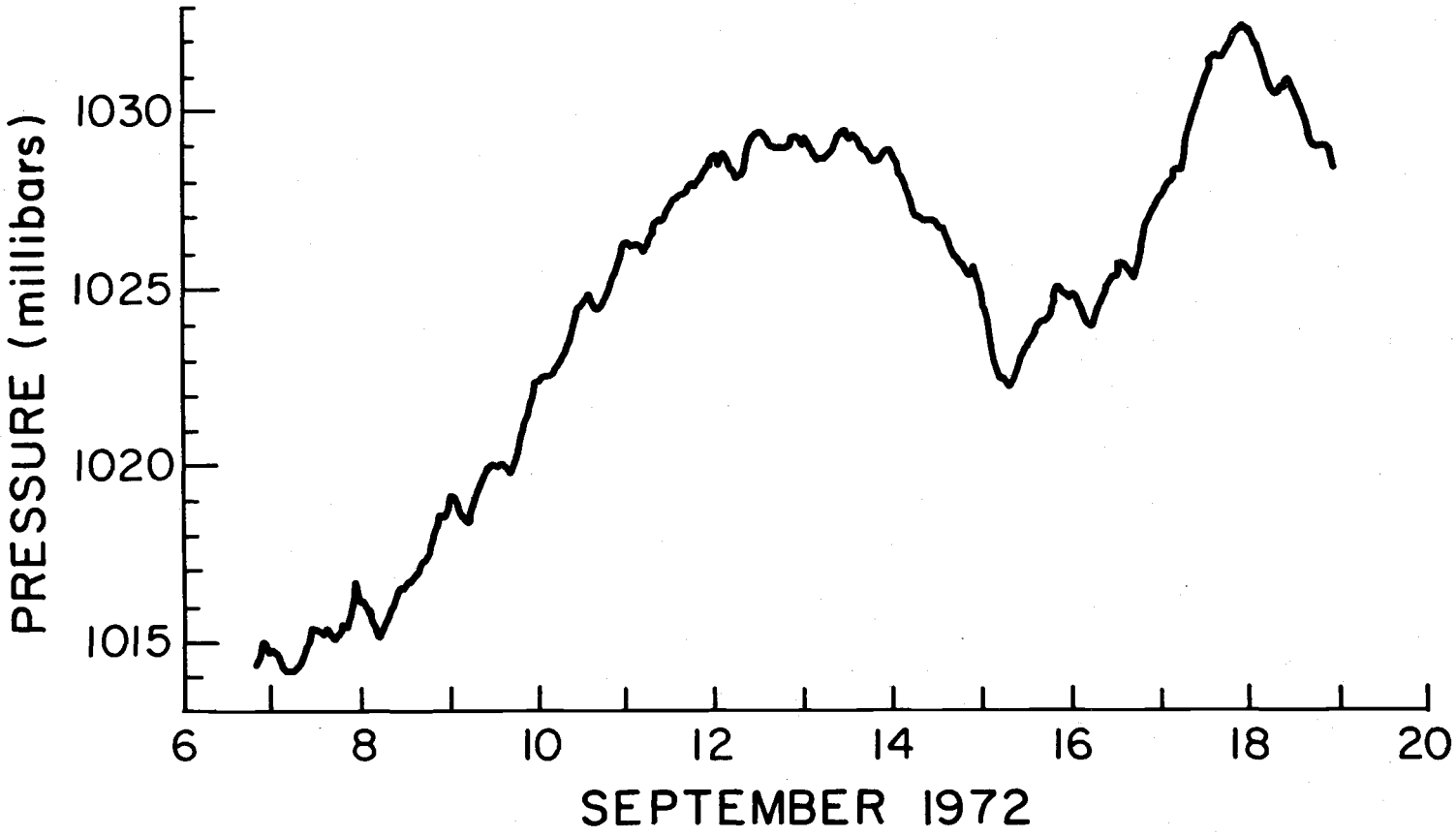

Figure 13. Time series of hourly air pressure data from M/V Researcher.

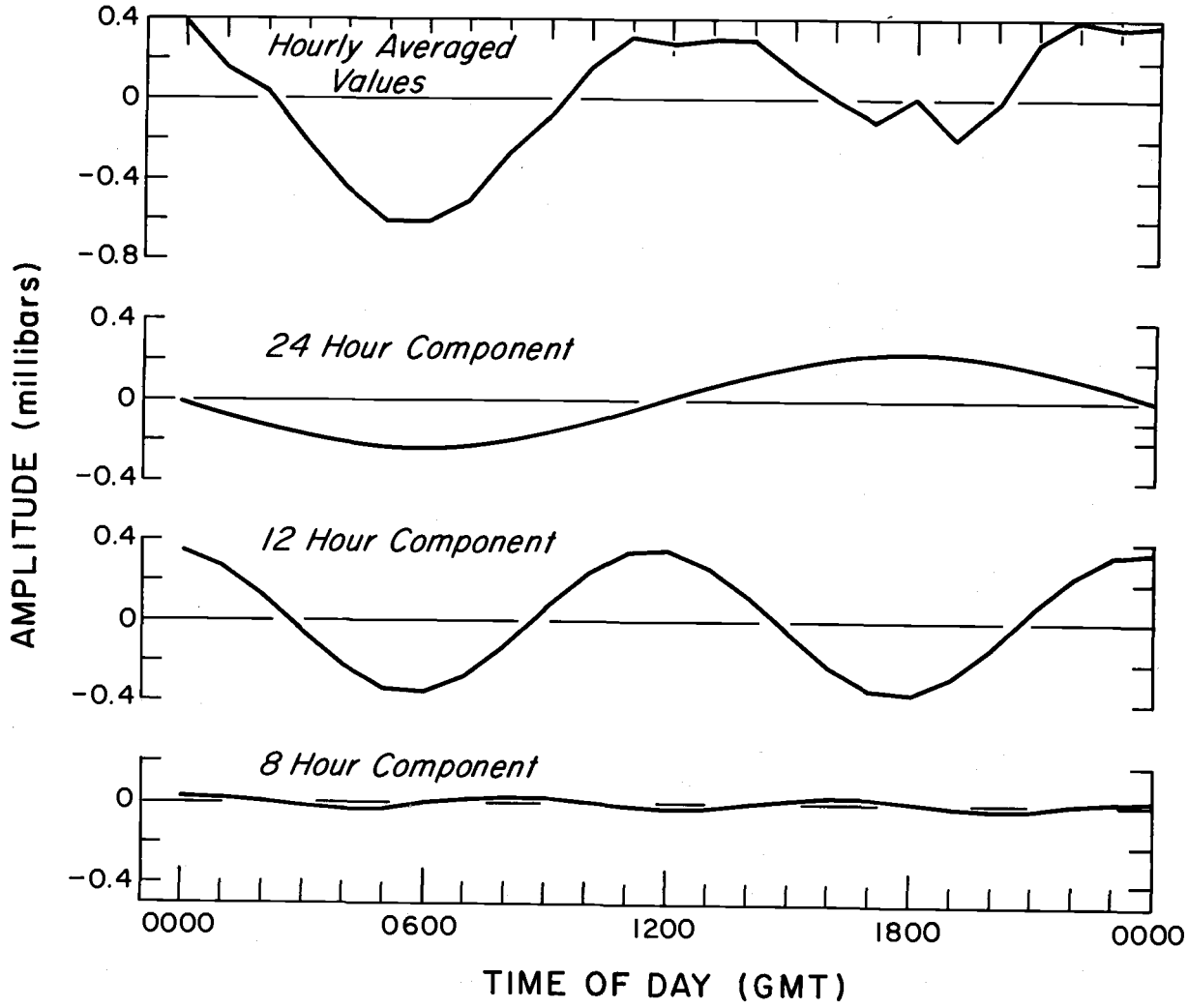

Figure 14. Harmonic analysis of air pressure data from M/V Researcher for 24, 12, and 8 hour components.

discussed due to its possible similarity with divergence.

The eight hour wave is not predicted from gravitational theory as the 24 and 12 hour waves are but appears as a progressive wave of strange symmetry (Bartels, 1938). For two stations in the northern hemisphere Bartels (1932) found that the first maxima in the wave during the winter months occurs shortly after 0200 local time, with the first minima four hours later. During the summer months this wave will be reversed with the first maxima shortly after 0600 local time and the first minima four hours earlier. Bartels indicates two possible causes of the eight hour wave. First, he mentions that the eight hour wave of temperature exhibits similar reversals indicating a cause and effect relation between the eight hour wave of pressure and temperature. Then he shows a chart giving the horizontal air-movements in the atmosphere which would accompany the eight hour wave of pressure. It is this progressive wave moving towards the west around the earth that he believes could also cause the pressure changes evident in the eight hour wave.

The phase and amplitude of the eight hour pressure wave are almost independent in relation to location from the sea (Bartels, 1938). This would indicate that altitude and horizontal distance from a coast-line have little effect on this wave. This would allow for comparison between the ocean station data of this study and the land station data of previous authors.

The harmonic analysis for the M/V Researcher pressure data shows very strong 24 and 12 hour components. The eight hour wave seems small in comparison to the others but it agrees quite well with observations by Bartels (1938) both in magnitude and phase. The divergence record was too rough to pick out any similarities in phase between zero divergence and a maximum or minimum in the magnitude of the eight hour pressure wave. The existence of an eight hour pressure wave and a possible eight hour component in divergence does indicate the possibility of some relationship since the pressure wave could be accompanied by rising or sinking air, which could also come with converging or diverging air.

One may expect 24 and 12 hour components of the divergence to correlate with the corresponding 24 and 12 hour components of pressure. This is not the case since the spectral plot of divergence does not show any significant peaks at those periods. This appears to substantiate the theory that a component of divergence is possibly related to the eight hour pressure wave, which in turn is related to the eight hour temperature wave. The 24 and 12 hour pressure waves are gravitational waves which have no apparent effect on the divergence.

As a follow-up to the above analysis, linear correlations were done for hourly values between 17 kilometer divergence (illustrated in Figure 15a) and 100 kilometer divergence, 17 kilometer vorticity

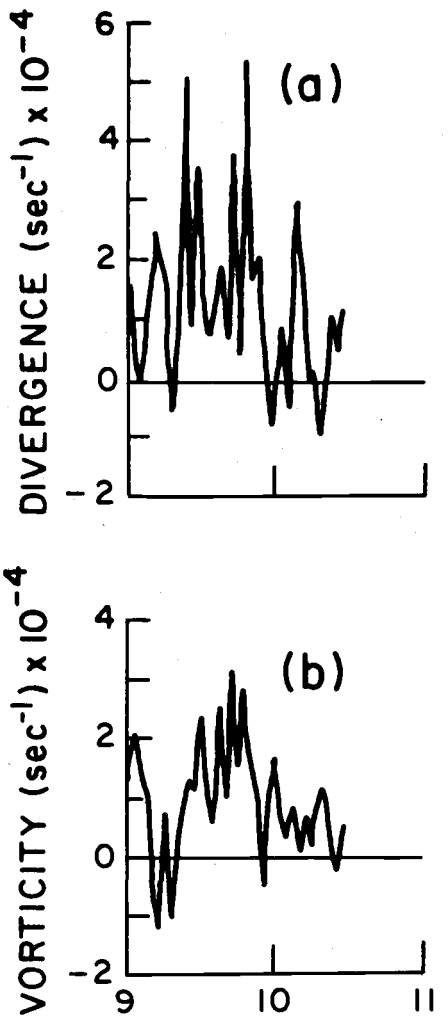

Figure 15. Time series of (a) hourly divergence estimates and (b) hourly vorticity estimates from 17 km triangle.

(illustrated in Figure 15b) and 100 kilometer vorticity, 17 kilometer vorticity and Researcher pressure, 100 kilometer vorticity and Researcher pressure, 17 kilometer divergence and Researcher pressure, 100 kilometer divergence and 100 kilometer vorticity, and 17 kilometer divergence and 17 kilometer vorticity. Where the 17 kilometer grid was involved there were only 36 points, while if Researcher pressure was involved, there were 293 points. Otherwise, there were a full 303 points. At the same time that linear correlation coefficients were computed means and standard deviations were also computed (Table 3). Records with 36 points cover the period from 0000 GMT 9/9/72 to 1100 GMT 9/10/72. Records with 293 points cover the period from 1900 GMT 9/6/72 to 2300 GMT 9/18/72. Records with 303 points cover the period from 1900 GMT 9/6/72 to 0900 GMT 9/19/72. Linear correlation coefficients are given in Table 4.

Table 3. Means and standard deviations of divergence, vorticity, and pressure data.

	N	Mean	Standard Deviation
17 km vorticity	36	9.12×10^{-5} sec^{-1}	9.93×10^{-5}
17 km divergence	36	1.27×10^{-4} sec^{-1}	1.51×10^{-4}
Researcher pressure	293	1024.59 mb	60.18
100 km vorticity	303	-1.57×10^{-5} sec^{-1}	2.32×10^{-5}
100 km divergence	303	1.14×10^{-5} sec^{-1}	2.02×10^{-5}

Table 4. Linear correlation coefficients between divergence, vorticity, and pressure data.

	N	Linear Correlation Coefficient
17 km vorticity x 17 km divergence	36	.30
100 km vorticity x 100 km divergence	303	.10
17 km divergence x 100 km divergence	36	.74
17 km vorticity x 100 km vorticity	36	.63
17 km vorticity x Researcher pressure	36	-.14
17 km divergence x Researcher pressure	36	-.29
100 km divergence x Researcher pressure	293	-.31
100 km vorticity x Researcher pressure	293	-.31

In examining the linear correlations, it is found that there are poor correlations between Researcher pressure and divergence or vorticity for both grids. This is not surprising, since it has been shown previously that one frequency component of pressure (eight hour period) possibly correlates with divergence, while not at all with vorticity. Correlations between divergence and vorticity for each grid are also quite low. This may indicate that rising or sinking air was not a function of whether the JASIN area with its small horizontal pressure gradients during the time of observation was experiencing cyclonic or anticyclonic motion. The only fair correlations are for vorticity between the two grids and divergence between the two grids.

This shows that there was some continuity of divergence and vorticity on a horizontal scale over the ocean area under study at the time the observations were made. In examining the means of vorticity and divergence for both grids it is shown that the smaller grid has values approximately an order of magnitude larger than those of the larger grid. The comparison of standard deviations between the two grids for divergence and vorticity follows in the same way. The orders of magnitude of these means of vorticity and divergence also compare favorably with values determined by Petterssen (1956) and Haltiner and Martin (1957).

V. CONCLUSIONS

During the planning stages of this study, it was thought that the absence of the disturbing influences of topography over the ocean would cause more homogeneity or horizontal continuity in the wind field over the oceans than had been found in previous studies over land. The fact that the JASIN study area did not have any strong weather disturbances and the wind velocity was rather low, during the study period, would tend to strengthen the above thought.

The various analyses of the wind field, during JASIN, did show many similarities over the 100 km area under study. However, there were some surprising and striking differences displayed in the data.

The wind data from Buoy A (Figure 1) was most surprising, since it showed some radical differences from the data from the other buoys. It was surprising that points, only 100 km apart, in a rather flat, relatively undisturbed pressure field, could display different wind fields.

The power spectra of the horizontal wind field showed similar patterns at the various sampling stations and compared favorably with the composite spectrum of Millard (1968). However, there were small differences between the spectra from Buoys B1, B2, D1, and D2 with a markedly different spectrum at Buoy A. There were slightly lower energy levels in the mesoscale frequency range in the JASIN

wind spectra as compared to Millard's spectrum.

Progressive vector diagrams of the wind at Buoys B1 and D2 show differences in wind direction that cannot be explained by any constant error in the direction measurements. It would appear that rather large differences in direction and speed can be expected over the ocean in distances as short as 17 kilometers. The progressive wind vector diagrams from the more widely spaced buoys showed even greater variation between the data from the various buoys.

Perhaps the large changes in the wind field over the area studied are best illustrated in Figure 8 that shows the mean diurnal cycles in changes in both wind speed and direction for the 13 day period of common record at four different locations. Data from Buoys B1 and D2 showed mean wind vectors to the northwest, while the mean vectors for Buoys B2 and A data was to the southeast, with the vector for the A data being more than double that of the B2 data.

Because of the configuration of the locations of the buoys, vorticity and divergence estimates were possible over two subscales of the mesoscale. Computations of vorticity confirmed that the area was in a zone of cyclonic motion, except for the period of two days centered around midnight of the 10th of September. Strangely the cyclonic motion, during the period of observation, does not appear in the published surface synoptic analysis charts for the JASIN area. It would appear that a zone of cyclonic motion to the northeast

extended into the JASIN area, but was not detected by individuals drawing the surface maps due to the rather flat pressure field that extended over the JASIN area most of the month of September.

A curious eight hour period was found in the divergence records for the 100 km triangle, which is possibly related to an eight hour surface air pressure wave that was studied many years ago, but has since been forgotten (Chapman, 1951; and Bartels, 1938). It should be noted that the aliasing of wind direction and buoy motion is a possible cause of the peak in the divergence spectra in the eight to ten hour range period.

The 1/L relationship mentioned earlier was roughly proven for both divergence and vorticity, but should be studied further with buoy arrays with larger numbers of buoys.

BIBLIOGRAPHY

American Meteorological Society. 1971. Conference on the interaction of the sea and the atmosphere. Ft. Lauderdale, Fla. Dec. 1-3, 1971.

Ballance, J., J. Baughman, and L. Ochs. 1971. OS-3 ARAND system: documentation and examples. Vol. 2. OSU Computer Center. CCR-71-01. 238 p.

Bartels, J. 1932. Tides in the atmosphere. In: The Magnetic Field of the Earth and Its Atmosphere. Carnegie Institution of Washington. Supplementary Publications No. 5. pp. 48-68.

_____ 1938. Sonnen-und mondentägige luftdruckschwankungen. Lehrbuch der meteorologie. Hann-Süring. 5. Aufl., Bd. I. Leipzig. W. Keller. pp. 276-306.

Bendat, J. S. and A. G. Piersol. 1971. Random data: analysis and measurement procedures. John Wiley & Sons, Inc. 407 p.

Chapman, S. 1951. Atmospheric tides and oscillations. In: Compendium of Meteorology. Edited by T. F. Malane. American Meteorological Society. pp. 510-530.

Cummings, T. 1973. Unpublished computer programs.

Fiedler, F. and H. A. Panofsky. 1970. Atmospheric scales and spectral gaps. Bulletin of the American Meteorological Society. 51(12). pp. 1114-1119.

Gray, W. M. 1972. Cumulus convection and larger-scale circulations. Part III. Broadscale and mesoscale considerations. Atmospheric Science Paper No. 190, Dept. of Atmos. Sci. Colorado State Univ. 80 p.

Haltiner, G. J. and F. L. Martin. 1957. Dynamical and physical meteorology. McGraw-Hill Book Co. 470 p.

Hsueh, Y. 1968. Mesoscale turbulence spectra over the Indian Ocean. Journal of the Atmospheric Sciences. 25(6). pp. 1052-1057.

Lettau, H. 1973. Personal communication with W. V. Burt. 2 p.

Millard, R. C. 1971. Wind measurements from buoys: a sampling scheme. Journal of Geophysical Research. 76(24). pp. 5819-5828.

Ochs, L., J. Baughman, and J. Ballance. 1970. OS-3 ARAND system: documentation and examples. Vol. 1. OSU Computer Center. CCR-70-4. 158 p.

Panofsky, H. A. 1946. Methods of computing vertical motion in the atmosphere. Journal of Meteorology. 3(2). pp. 45-49.

Petterssen, S. 1956. Weather analysis and forecasting. Vol. 1. Motion and motion systems. McGraw-Hill Book Co. 428 p.

Pollard, R. T. 1972. Personal communication with W. V. Burt. 19 p.

Royal Society, The. 1971. Royal Society Air-Sea Interaction Project. 1970 Trial-Operation JASIN (12 to 22 June 1970) Cruise Report. 70 p.

Roll, H. U. 1971. Air-sea interaction in the different scales of motion. Lecture given at the Air-Sea Interaction Conference at Fort Lauderdale, Fla., on December 1, 1971. 18 p.

Schaefer, J. T. 1973. On the computation of the surface divergence field. Journal of Applied Meteorology. 12(3). pp. 546-547.

Streeter, V. L. 1966. Fluid mechanics. 4th Ed. McGraw-Hill Book Co. 705 p.

Von Hann, J. 1918. Untersuchungen über die tägliche oszillation des barometers. Die dritteltagige (achtstundige) luftdruck-schwankung. Denkschr. Akad. Wiss. Wien. Vol. 95. pp. 1-64.

World Meteorological Organization. 1972. Experiment design proposal for the GARP Atlantic Tropical Experiment. GATE Report No. 1. Global Atmospheric Research Program (GARP). 188 p.

APPENDIX

APPENDIX

Computer Programs

1. Program VORT. This program computes the divergence and vorticity for an equilateral triangle grid.

```
      PROGRAM VORT
C***** PROGRAM TO COMPUTE THE VORTICITY AND DIVERGENCE
C***** IN AN EQUILATERAL BUOY ARRANGEMENT.
      DIMENSION ITIME(4), FORM(10), WS(3), WD(3), VWD(3), U(3), V(3)
      NPTS=DECIN(4HNUMB, 4HER 0, 4HF PO, 4HINTS, 4H=    )
      KK=INCHAR(FORM, 4HINPU, 4HT FO, 4HRMAT, 4H IS., 4H....)
      CORR=DECIN(4HCORR, 4HECTI, 4HON A, 4HNGLE, 4H FOR, 4H GRI, 4HD = )
      Y=DECIN(4HLENG, 4HTH 0, 4HF SI, 4HDE(M, 4HETER, 4HS)= )
      X=SQRT(Y**2-(.5*Y)**2)
      KOUNT=0
      DO 100 I=1, NPTS
      READ(1, FORM)(ITIME(J), J=1, 4), ((WS(K), WD(K)), K=1, 3)
      DO 20 K=1, 3
      VWD(K)=WD(K)+CORR
      IF(VWD(K).GT.360.)VWD(K)=VWD(K)-360.
      VWD(K)=.017453*VWD(K)
      U(K)=WS(K)*SIN(VWD(K))
      V(K)=WS(K)*COS(VWD(K))
20    CONTINUE
      VOR=(((V(2)+V(3))/2.)-V(1))/X-(U(2)-U(3))/Y
      DIV=(((U(2)+U(3))/2.)-U(1))/X+(V(2)-V(3))/Y
      KOUNT=KOUNT+1
      WRITE(2, 10)(ITIME(J), J=1, 4), VOR, DIV, KOUNT
10    FORMAT(4A4, 2E10.2, I6)
100   CONTINUE
      ENDFILE 2
      END
```

2. Program DIVCONV. This program computes the divergence for a polygonal buoy arrangement.

```
      PROGRAM DIVCONV
C***** PROGRAM TO COMPUTE THE DIVERGENCE IN A POLYGONAL BUOY
C***** ARRANGEMENT.  THE NORMAL WIND VECTORS(POSITIVE OUTWARDS)
C***** FOR EACH FACE OF THE POLYGON AT EACH BUOY ARE COMPUTED.
C***** A NORMAL WIND VECTOR IS FOUND FOR EACH FACE BY AN AVERAGE
C***** OF THE TWO NORMAL VECTORS BOUNDING EACH FACE.  EACH VECTOR
C***** IS MULTIPLIED BY THE LENGTH OF ITS RESPECTIVE SIDE THEN ALL
C***** IS SUMMED.  THE DIVERGENCE IS THIS SUM DIVIDED BY THE AREA
C***** OF THE POLYGON.
      DIMENSION ITIME(4), DIR(99), VDIR(99, 2), WS(99), VA(99, 2), V(99)
      DIMENSION FORM1(10), FORM2(10), CORR(99), FL(99)
      KK=INCHAR(FORM1, 4HINPU, 4HT FO, 4HRMAT, 4H IS., 4H....)
      KK=INCHAR(FORM2, 4HOUTP, 4HUT F, 4HORMA, 4HT IS, 4H....)
      NFACES=DECIN(4HNUMB, 4HER 0, 4HF FA, 4HCES , 4HIN P, 4HOLYG, 4HON= )
      NLINES=DECIN(4HLINE, 4HS OF, 4H DAT, 4HA=  )
      AREA=DECIN(4HAREA, 4H OF , 4HPOLY, 4HGON(, 4HMETE, 4HRS**, 4H2)= )
      DO 10 I=1, NFACES
      WRITE(61, 4)I
4     FORMAT(' LENGTH OF FACE ', I2, ' IN DEGREES ')
      FL(I)=DECIN(4H....)
      WRITE(61, 6)I
6     FORMAT(' CORRECTION ANGLE FOR FACE ', I2, ' IN DEGREES ')
      CORR(I)=DECIN(4H....)
10    CONTINUE
      KOUNT=0
      DO 100 I=1, NLINES
      READ(1, FORM1)(ITIME(J), J=1, 4), ((WS(K), DIR(K)), K=1, NFACES)
      DIV=0.
      DO 90 J=1, NFACES
      DO 89 K=1, 2
      L=J
      II=K.EQ.2
      JJ=J.EQ.NFACES
      IF(II)L=J+1
      IF(II.AND.JJ)L=1
      VDIR(J, K)=DIR(L)+CORR(J)
      IF(VDIR(J, K).GT.360.)VDIR(J, K)=VDIR(J, K)-360.
      VDIR(J, K)=.017453*VDIR(J, K)
      VA(J, K)=WS(L)*COS(VDIR(J, K))
89    CONTINUE
      V(J)=(VA(J, 1)+VA(J, 2))/2.
      DIV=DIV+(V(J)*FL(J))
90    CONTINUE
      KOUNT=KOUNT+1
      DIV=DIV/AREA
      WRITE(2, FORM2)(ITIME(J), J=1, 4), DIV, KOUNT
100   CONTINUE
      ENDFILE 2
      END
```